Reversible Iodine Intercalation into Tungsten Ditelluride

Patrick Schmidt,[a] Philipp Schneiderhan,[a] Markus Ströbele,[a] Carl P. Romao,[a]* H.-Jürgen Meyer[a]*

Abstract: The new compound WTe_2I was prepared by a reaction of WTe_2 with iodine in a fused silica vessel at temperatures between 40 and 200 °C. Iodine atoms are intercalated into the van der Waals gap between tungsten ditelluride layers. As a result, the WTe_2 layer separation and therefore the *c*-axis length is significantly increased, and the orthorhombic space group is preserved. Iodine atoms form planar layers between each tungsten ditelluride layer. Due to oxidation by iodine the semi-metallic nature of WTe_2 is changed, as shown by comparative band structure calculations for WTe_2 and WTe_2I based on density functional theory. The calculated phonon band structure of WTe_2I suggests a charge density wave instability at low temperature.

Introduction

Transition metal dichalcogenides (TMDCs) are quasi-two-dimensional layered materials, formed by monolayers of metal atoms sandwiched between layers of chalcogen atoms. Weak van der Waals interlayer bonding between building blocks of hexagonal chalcogen layers with nearly octahedral or nearly trigonal prismatic metal atoms allow many polytypes to form.[1] The weak interlayer bonding permits intercalations, quite akin to other layered materials such as graphite,[2] allowing the incorporation of various metal atoms[3] and organic molecules[4] between the layers to form stoichiometric or nonstoichiometric compounds. Depending on the intercalated species, changes in the physical properties of the host can occur. In addition, such intercalated species can be used as precursors for the exfoliation of single TMDC layers.[5]

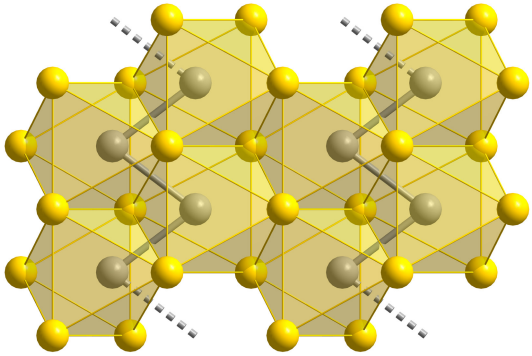

Figure 1. Projection of the WTe_2 structure. View along the *c*-axis of the distorted T_d structure in which tungsten (grey) atoms follow a CDW along the *a*-axis. Tungsten atoms are shifted off the octahedral centers formed by tellurium (yellow) atoms.

* Prof. Dr. H.-J. Meyer,
[a] Section of Solid State and Theoretical Inorganic Chemistry
Institute of Inorganic Chemistry
Eberhard Karls University Tübingen
Auf der Morgenstelle 18
72076 Tübingen, Germany
E-Mail: juergen.meyer@uni-tuebingen.de

Tungsten ditelluride (WTe_2)[6] is a typical TMDC that crystallizes with the so-called distorted 1T (T_d) structure. The structure resembles a distorted derivative of TiS_2[7] with distorted tellurium octahedra and tungsten atoms shifted away from octahedral centers, thereby forming zigzag chains along the *b*-axis direction (**Figure 1**). The arrangement of tungsten atoms in the structure plays a significant role in the remarkable electronic properties of WTe_2. Electronic structure calculations have revealed WTe_2 to be a semi-metal.[8] Physical studies have revealed many excellent properties for WTe_2, including charge density wave (CDW)[9] formation, superconductivity,[10] large magnetoresistance[11] and the presence of nontrivial topological properties such as the appearance of type-II Weyl fermions,[12] making this material interesting for a variety of electronic applications. The oxidation of WTe_2 with iodine and the formation of the intercalated species WTe_2I modifies the electronic structure and therefore changes the properties of this material. Moreover, this type of anionic intercalation has not been reported before in a TMDC, according to our knowledge, and may be applicable to other TMDC systems as well.

Results and Discussion

Reactions of metal dichalcogenides with halides have been reported to yield mixed chalcogenide-halide cluster compounds. An example is the formation of $Re_3Se_2Br_5$ from $ReSe_2$ with Br_2 (at 450 °C).[13] Following this example we have explored the reaction of WTe_2 with iodine. WTe_2 can be prepared from well-known transport reactions of the elements in fused silica tubing, like other transition metal chalcogenides.[6, 8a, 14] A detailed study of the reaction of WTe_2 with iodine in a fused silica ampoule reveals several reaction steps with increasing temperature and iodine pressure. The first step is an intercalation of iodine into interlayers of the WTe_2 structure, yielding the new compound WTe_2I, which occurs following heating above 40 °C in a closed vessel. When heated above 200 °C, iodine and TeI_4 are released until $(TeI_3)_2[W_6I_{14}]$ is formed at 250 °C.[15]

A chemical analysis of WTe_2I by inductively coupled plasma optical emission spectrometry (ICP-OES) confirmed the identity of the product with resulting averaged ratios of elements corresponding to W : Te : I = 1 : 1.98 : 0.99.

The crystal structure of WTe_2I, as refined from X-ray powder diffraction data, is closely related to that of WTe_2, both crystallizing with the same orthorhombic space group (**Table 1**). Individual WTe_2 layers and corresponding W–W and W–Te distances remain almost unchanged before and after the reaction with I_2 (**Table 1**). However, the *c*-axis of the unit cell increases by approximately 50% (**Table 1**) due to the intercalation of iodine atoms between adjacent WTe_2-layers. The orientation of the WTe_2 layers in the *ab*-plane changes by

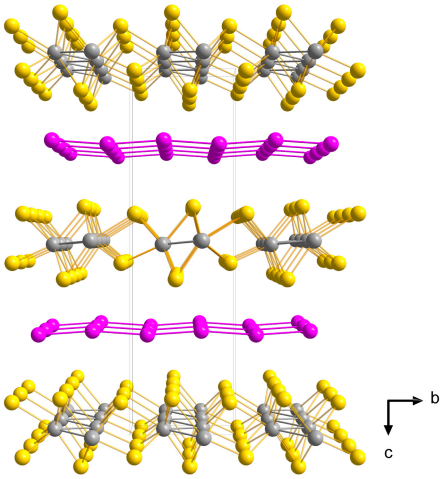

Figure 2. Projection of the crystal structure of WTe_2I, showing a layered arrangement. Tungsten atoms are shown grey, iodine violet and tellurium atoms yellow.

moving every second layer in opposite *b*-directions so that the tungsten chains are aligned along the *c*-axis (**Figure 2**).

Table 1. Crystallographic data, and W–W and W–Te distances of WTe_2 and WTe_2I.

	WTe_2[16]	WTe_2I
Space group	$Pmn2_1$	$Pmn2_1$
a / Å	3.477(2)	3.4736(1)
b / Å	6.249(4)	6.3236(1)
c / Å	14.018(9)	21.8818(3)
V / Å^3	304.6(3)	480.66(1)
d(W–W) / Å	2.85(1), 3.48(1)	2.88, 3.47
d(W–Te) / Å	2.70(1)–2.80(1)	2.66–2.90

Iodine atoms form nearly rectangular, planar layers within the *ab*-plane with I–I distances of 3.14 Å and 3.47 Å. A similar arrangement of iodine layers with values of 3.32 and 3.84 Å was reported in the unusual intercalation compound $(Te_2)_2(I_2)$[17]. Another, more closely related, TMDC intercalation compound containing a planar iodine network is $AuTe_2I$[18], which has I–I distances of 4.06(1) and 4.74(1) Å.

As noted above, the incorporation of iodine atoms into the structure of WTe_2 yields a significant increase of the interlayer distances (increase from 7.052 Å in WTe_2 to 10.943 Å in WTe_2I). This increase is huge compared to cationic

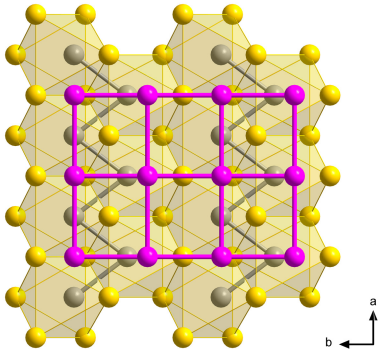

Figure 3. Arrangement of a rectangular net of iodine atoms on top of a WTe_2 layer of the WTe_2 structure (W = grey, Te = yellow, I = violet).

intercalation compounds like in WS_2In (increasing from 6.162 Å in WS_2 to 6.183 Å in WS_2In).[19] As a result of this strong interlayer expansion and weak interaction forces between layers, dislocations are typically obtained (see **Figure S1**).

The intercalation reaction between iodine and WTe_2 under autoclave conditions proceeds without a detectable calorimetric effect. The deintercalation of iodine from WTe_2I under ambient pressure can be observed above 100 °C (**Figure 4**). The observed exothermic effect corresponds to the sublimation energy of the released iodine (in a constant argon flow) and has no correlation with the intercalation energy.

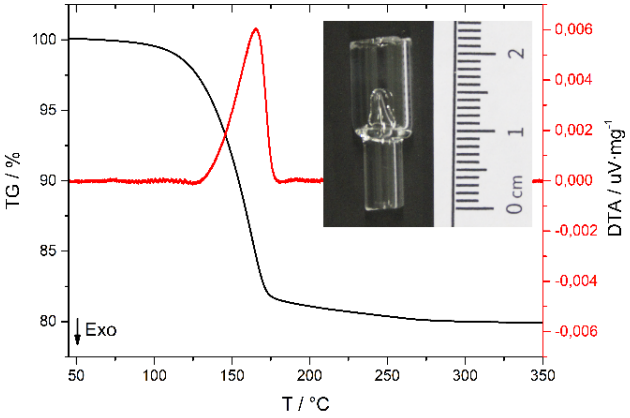

Figure 4. DTA/TG measurement of WTe_2I in an open SiO_2 container up to 350 °C with complete iodine loss (DTA: red line, TG: black line).

Electronic structure

The calculated electronic band structure of WTe_2I is shown in **Figure 5**. Comparison to the band structure of WTe_2 (**Figure 6**) shows that the addition of iodine layers to the structure increases the density of states (DOS) at the Fermi level significantly, leading to a transition from a semimetal to a metal. These additional states are largely located between the Γ ([0 0 0]), Z ([0 0 ½]), and Y ([0 ½ 0]) points in reciprocal space. The projected density of states shows that the states around the Fermi level have contributions from W, Te, and I atoms; many of the states project onto interatomic regions which cannot be assigned to a single atom.

Along the Γ–X–U–Z–Γ path in reciprocal space (**Figure 5**), the calculated band structure of WTe_2I closely resembles that of WTe_2 with the Fermi level shifted downwards by approximately 0.5 eV. The significant increase in the DOS at the Fermi level following the addition of iodine can therefore be partially attributed to the depletion of some electron density from the tungsten telluride layers into the iodine layers. In WTe_2, an avoided crossing of two bands due to spin-orbit coupling near the Fermi level along the Γ–X direction gives rise to Weyl semimetal behavior.[12, 20] The addition of iodine to form

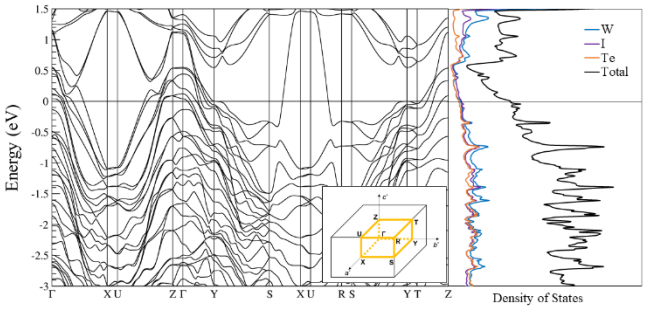

Figure 5. The electronic band structure and density of states of WTe_2I, calculated with spin-orbit coupling. The projected densities of states within the PAW spheres are shown as coloured lines at right. Special points in the Brillouin zone are shown as an inset.

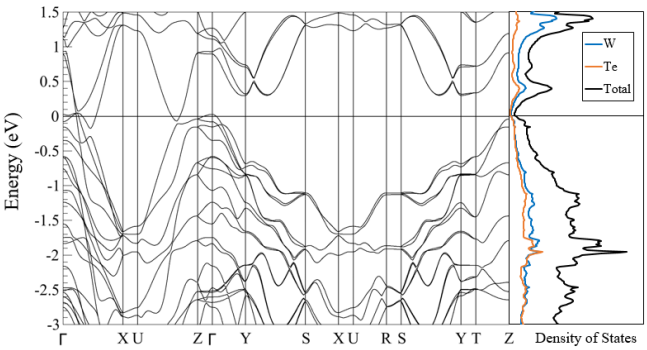

Figure 6. The electronic band structure and density of states of WTe_2, calculated without spin-orbit coupling (see Ref. [8c] for the band structure with spin-orbit coupling). The projected densities of states within the PAW spheres are shown as coloured lines at right.

WTe_2I moves the Fermi level away from this feature, into a region with more conventional bands at the Fermi surface.

The addition of iodine to WTe_2 also creates additional bands at the Fermi level between S ([½ ½ 0]) and X ([½ 0 0]) and between U ([½ 0 ½]) and R (compare **Figure 5** and **Figure 10**). These bands have very high dispersion, indicating small effective electron masses and large charge carrier mobility. They are associated with Dirac cone-like anticrossings lying approximately 0.5 eV below the Fermi level. Several methods were used to investigate the nature of these highly dispersive

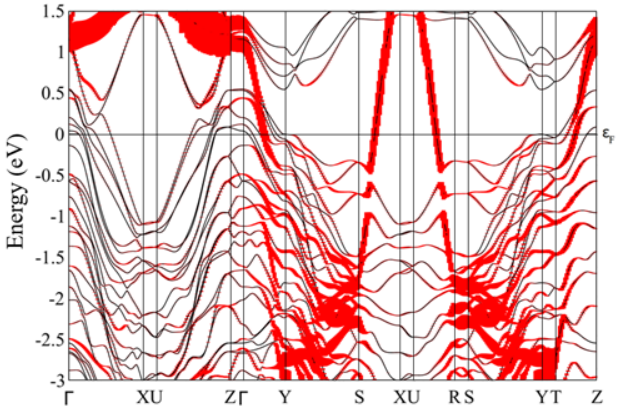

Figure 7. Projected contributions of p_y spherical harmonics to electronic bands in WTe_2I, shown in red as fatbands.

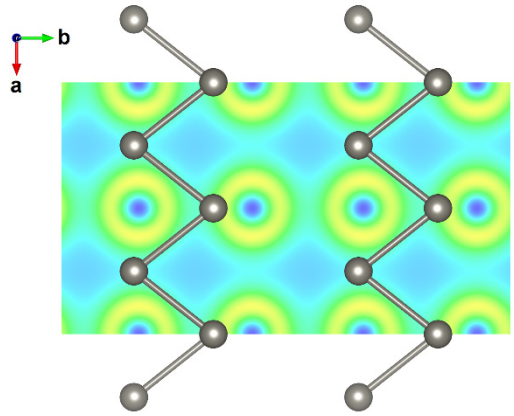

Figure 8. The density of valence electrons, in a section through iodine atoms in the ab plane. The W atoms above the plane are shown for comparison.

bands. Projections of the wavefunctions near each atom onto spherical harmonics were used to determine the atomic and orbital character of the wavefunctions corresponding to the bands. As shown in Figure Z, this indicated that the bands of interest can be largely assigned to iodine p_y orbitals. To validate this result, the electronic band structure of the iodine layer alone was calculated, and the features between S and X and U and R can also be found there (**Figure 10**).

Examination of the electron density around the iodine atoms (**Figure 8**) shows some evidence of bonding (*i.e.*, interstitial electron density) in chains along *b*. Stronger bonding is indicated between iodine atoms with an interatomic distance of 3.14 Å in the crystal structure. The formation of dimers along *b* indicates that the bands with p_y character (**Figure 8**) correspond to σ bonding and antibonding orbitals.

The effect of these modifications of the structure and Fermi surface was assessed by calculation of the phonon band structure (**Figure 9**). Several soft modes (modes with imaginary frequencies, shown as negative values in **Figure 9**) are present. These modes correspond to instabilities of the room temperature structure which would appear upon cooling (as the calculated phonon band structure corresponds to 0 K). They can be identified as Kohn anomalies, that is, they cause the formation of charge density waves (CDW) and a consequent symmetry-lowering phase transition on cooling.[1a] The Kohn anomalies are related to nesting vectors of the Fermi

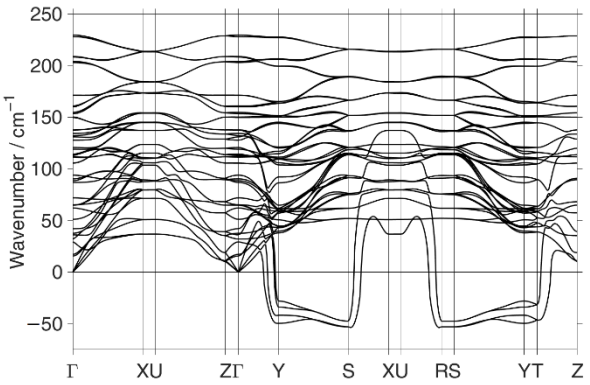

Figure 9. The calculated phonon band structure of WTe_2I.

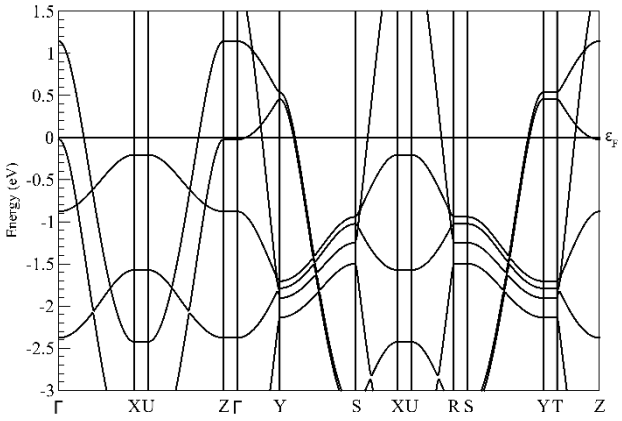

Figure 10. The electronic band structure of the iodine layers in WTe_2I.

surface; the introduction of additional bands crossing the Fermi level therefore opens new possibilities for such nesting. The phonon band structure also shows numerous triply-degenerate nodal points between S and X and U and R, where optic bands invert and become lower in energy than the acoustic bands. These topological features can act as additional phonon scattering centers and lead to glass-like thermal conductivity.[21] There are also numerous crossings and near-

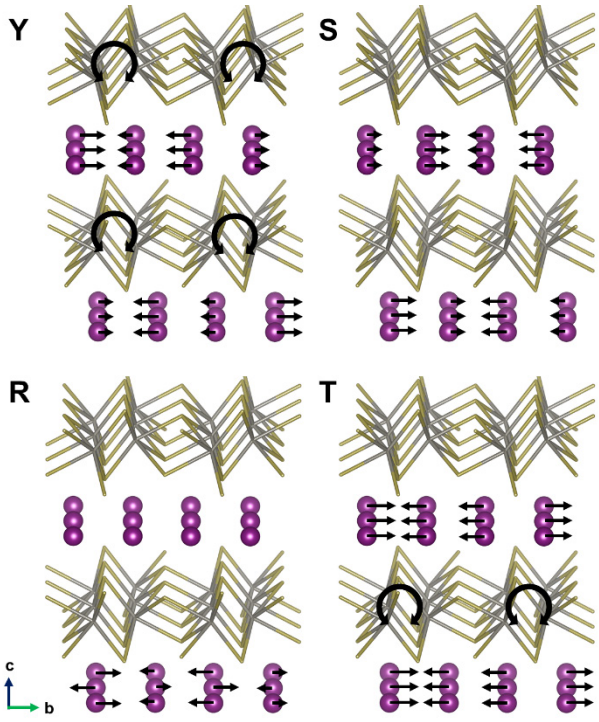

Figure 11. A cartoon view of several soft modes in WTe_2I. The modes with the largest imaginary frequency (most negative values in **Figure 8**) at the Y, S, R, and T points are shown. Linear oscillations of I atoms are shown as black arrows, and rocking motions of the WTe_2 layers are shown as curved arrows.

crossings of bands, especially near Γ, which may correspond to topologically charged Weyl phonons.[21]

The nature of the CDW can be determined by examination of the eigenvectors of the soft modes, which are shown in cartoon form in **Figure 11**. These modes all involve oscillations of iodine atoms along b, with rocking motions of the WTe_2 layers being incorporated in some cases. Due to the large number of soft modes, the phase which is formed upon cooling cannot be predicted from this data. Formation of a disordered or incommensurately modulated phase is certainly possible given the shallowness of the potential energy surface between the various soft modes.

Conclusions

The crystal structure of tungsten ditelluride and various properties have been well studied. Although intercalation compounds of WTe_2 with alkali ions are known, no crystal structures has been reported in ICSD.[22] Herein we present the reversible intercalation of iodine into the structure of WTe_2, and we report the crystal structure of WTe_2I. In the light of the many interesting physical properties of WTe_2, this intercalate with an oxidized tungsten species represents an interesting material. Electronic band structure calculations reveal a metallic behavior of WTe_2I, revealing steep bands with dominant iodine p-band character crossing the Fermi level. The phonon band structure indicates electronic instability within the iodine layers. Halogen intercalation is therefore demonstrated to present a potential method to reversibly modify the physical properties of WTe_2.

Experimental Section

Synthesis of WTe_2 and WTe_2I: Manipulations of starting materials were performed in an argon-filled glove box (MBraun, labmaster 130, O_2 < 1 ppm, H_2O < 1 ppm). WTe_2 was prepared in a dry, vacuum sealed silica ampoule with a 1:2 molar ratio of tungsten powder (ABCR GmbH, 99.95 %, 0.6–0.9 micron) and tellurium pieces (Evochem, 99.999 %) heated at 800 °C for 24 h (total mass 1 g). Additional 0.1 eq. WCl_6 (Arcos, 99.9+ %) has been added as an oxygen getter.
WTe_2I was prepared by heating a 1:2 molar mixture of WTe_2 and iodine (Honeywell, ≥99.8 %) in a dry, vacuum sealed silica ampoule at 100 °C for 16 hours. The product appeared as black powder.

Powder X-ray diffraction: PXRD patterns of products were collected with a Stadi-P (STOE, Darmstadt) powder diffractometer using germanium monochromated Cu-$K_{\alpha1}$ radiation (λ = 1.5406 Å) and a Mythen 1K detector.

ICP-OES: After dissolution of WTe_2I in 2-w% $NaOH/H_2O_2$ the W/Te/I ratio was determined by ICP-OES (iCAP 7400 Thermo Fisher Scientific).

Thermal Analysis: Differential thermal analysis (DTA) and thermal gravimetry (TG) measurements were performed with a Netzsch Jupiter, STA 449 F3 apparatus between room temperature and 350 °C with a heating and cooling rate of 2

$K \cdot min^{-1}$ in homemade silica crucible (height: 2 cm, inner diameter 0.6 cm, thickness of wall: 0.1 cm).

DFT Calculations: Calculations were performed using the ABINIT software package with the projector augmented-wave (PAW) method and a plane-wave basis set.[23] The Perdew–Burke–Ernzerhof exchange–correlation functional was used with the vdw-DFT-D3 dispersion correction.[24] PAW data files were used as received from the ABINIT library.[25] Methfessel–Paxton smearing was used to determine band occupation.[26] Convergence studies and structural relaxation were performed prior to calculation of the electronic structure. Example input files are available as part of the ESI.

Acknowledgements

The authors appreciate the expertise and support of the following scientists from the University of Tübingen: Dr. Jochen Glaser for the ICP-OES.
Support of this research by the Deutsche Forschungsgemeinschaft (Bonn) through the project ME 914/31-1 and by the state of Baden-Württemberg through bwHPC and the German Research Foundation (DFG) through grant no INST 40/467-1 FUGG (JUSTUS cluster) are is gratefully acknowledged.

Conflict of interest

The authors declare no conflict of interest.

Keywords: tungsten chalcogenide • intercalation • synthesis • crystal structure • band structure • CDW • DTA

[1] a) G. H. Han, D. L. Duong, D. H. Keum, S. J. Yun, Y. H. Lee, *Chem. Rev.* **2018**, *118*, 6297-6336; b) M. J. Atherton, J. H. Holloway, in *Advances in Inorganic Chemistry and Radiochemistry, Vol. 22* (Eds.: H. J. Emeléus, A. G. Sharpe), Academic Press, **1979**, pp. 171-198; c) M. Chhowalla, *Nat. Chem.* **2013**, *5*, 263-275.

[2] H. P. Boehm, R. Setton, E. Stumpp, in *Pure Appl. Chem., Vol. 66*, **1994**, p. 1893.

[3] a) M. N. Ali, H. Ji, D. Hirai, M. K. Fuccillo, R. J. Cava, *J. Solid State Chem.* **2013**, *202*, 77-84; b) S. I. Ali, S. Mondal, S. J. Prathapa, S. van Smaalen, S. Zörb, B. Harbrecht, *Z. Anorg. Allg. Chem.* **2012**, *638*, 2625-2631; c) S. I. Ali, S. Mondal, S. van Smaalen, *Z. Anorg. Allg. Chem.* **2015**, *641*, 464-469; d) H. J. Crawack, C. Pettenkofer, *Solid State Commun.* **2001**, *118*, 325-332; e) J. Rouxel, *Physica B+C* **1980**, *99*, 3-11; f) S. N. Patel, A. A. Balchin, *J. Mater. Sci. Lett.* **1985**, *4*, 382-384.

[4] a) M. B. Dines, *Science* **1975**, *188*, 1210; b) E. Figueroa, J. W. Brill, J. P. Selegue, *J. Phys. Chem. Solids* **1996**, *57*, 1123-1127.

[5] a) P. Budania, P. T. Baine, J. H. Montgomery, D. W. McNeill, S. J. N. Mitchell, M. Modreanu, P. K. Hurley, *Micro Nano Lett.* **2017**, *12*, 970-973; b) A. Sajedi-Moghaddam, C. C. Mayorga-Martinez, E. Saievar-Iranizad, Z. Sofer, M. Pumera, *Appl. Mater. Today* **2019**, *16*, 280-289; c) G. Cunningham, M. Lotya, C. S. Cucinotta, S. Sanvito, S. D. Bergin, R. Menzel, M. S. P. Shaffer, J. N. Coleman, *ACS Nano* **2012**, *6*, 3468-3480; d) S.-J. An, Y. H. Kim, C. Lee, D. Y. Park, M. S. Jeong, *Sci. Rep.* **2018**, *8*, 12957; e) X. Liu, H. Chen, J. Lin, Y. Li, L. Guo, *Chem. Commun.* **2019**, *55*, 2972-2975; f) Y. Jung, Y. Zhou, J. J. Cha, *Inorg. Chem. Front.* **2016**, *3*, 452-463.

[6] B. E. Brown, *Acta Crystallogr.* **1966**, *20*, 268-274.

[7] R. R. Chianelli, J. C. Scanlon, A. H. Thompson, *Mater. Res. Bull.* **1975**, *10*, 1379-1382.

[8] a) S. Kabashima, *J. Phys. Soc. Japan* **1966**, *21*, 945-948; b) J. Augustin, *Phys. Rev. B* **2000**, *62*, 10812-10823; c) W. G. Dawson, D. W. Bullett, *J. Phys. C Solid State Phys.* **1987**, *20*, 6159-6174.

[9] a) C. Rovira, M. H. Whangbo, *Inorg. Chem.* **1993**, *32*, 4094-4097; b) J. A. Wilson, F. J. Di Salvo, S. Mahajan, *Adv. Phys.* **1975**, *24*, 117-201; c) M. N. Ali, *Nature* **2014**, *514*, 205-208; d) N. Lu, C. Zhang, C.-H. Lee, J. P. Oviedo, M. A. T. Nguyen, X. Peng, R. M. Wallace, T. E. Mallouk, J. A. Robinson, J. Wang, K. Cho, M. J. Kim, *J. Phys. Chem. C* **2016**, *120*, 8364-8369.

[10] C. Huang, A. Narayan, E. Zhang, Y. Liu, X. Yan, J. Wang, C. Zhang, W. Wang, T. Zhou, C. Yi, S. Liu, J. Ling, H. Zhang, R. Liu, R. Sankar, F. Chou, Y. Wang, Y. Shi, K. T. Law, S. Sanvito, P. Zhou, Z. Han, F. Xiu, *ACS Nano* **2018**, *12*, 7185-7196.

[11] Y.-Y. Lv, B.-B. Zhang, X. Li, B. Pang, F. Zhang, D.-J. Lin, J. Zhou, S.-H. Yao, Y. B. Chen, S.-T. Zhang, M. Lu, Z. Liu, Y. Chen, Y.-F. Chen, *Sci. Rep.* **2016**, *6*, 26903.

[12] P. Li, Y. Wen, X. He, Q. Zhang, C. Xia, Z.-M. Yu, S. A. Yang, Z. Zhu, H. N. Alshareef, X.-X. Zhang, *Nat. Commun.* **2017**, *8*, 2150.

[13] S. F. Solodovnikov, Y. V. Mironov, S. S. Yarovoi, A. V. Virovets, V. E. Fedorov, *Khim. Interesakh Ustoich. Razvit.* **2000**, *8*, 285–290.

[14] a) Y. Zhou, J. V. Pondick, J. L. Silva, J. M. Woods, D. J. Hynek, G. Matthews, X. Shen, Q. Feng, W. Liu, Z. Lu, Z. Liang, B. Brena, Z. Cai, M. Wu, L. Jiao, S. Hu, H. Wang, C. M. Araujo, J. J. Cha, *Small* **2019**, *15*, 1900078; b) L. H. Brixner, *J. Inorg. Nucl. Chem.* **1962**, *24*, 257-263; c) A. A. Al-Hilli, B. L. Evans, *J. Cryst. Growth* **1972**, *15*, 93-101; d) K. Ueno, *J. Phys. Soc. Jpn.* **2015**, *84*, 121015.

[15] P. Schmidt, A. Siai, P. Schneiderhan, M. Ströbele, H.-J. Meyer, *Eur. J. Inorg. Chem.* **2020**, in press.

[16] A. Mar, S. Jobic, J. A. Ibers, *J. Am. Chem. Soc.* **1992**, *114*, 8963-8971.

[17] R. Kniep, H.-J. Beister, *Angew. Chem. Int. Ed. Engl.* **1985**, *24*, 393-394.

[18] H. M. Haendler, D. Mootz, A. Rabenau, G. Rosenstein, *J. Solid State Chem.* **1974**, *10*, 175-181.

[19] S. K. Srivastava, B. N. Avasthi, *Synth. Met.* **1985**, *10*, 213-221.

[20] P. K. Das, D. Di Sante, F. Cilento, C. Bigi, D. Kopic, D. Soranzio, A. Sterzi, J. A. Krieger, I. Vobornik, J. Fujii, T. Okuda, V. N. Strocov, M. B. H. Breese, F. Parmigiani, G. Rossi, S. Picozzi, R. Thomale, G. Sangiovanni, R. J. Cava, G. Panaccione, *Electron. Struct.* **2019**, *1*, 014003.

[21] a) J. Li, Q. Xie, S. Ullah, R. Li, H. Ma, D. Li, Y. Li, X.-Q. Chen, *Phys. Rev. B* **2018**, *97*, 054305; b) S. Singh, Q. Wu, C. Yue, A. H. Romero, A. A. Soluyanov, *Phys. Rev. Mater.* **2018**, *2*, 114204.

[22] L. Zhu, Q.-Y. Li, Y.-Y. Lv, S. Li, X.-Y. Zhu, Z.-Y. Jia, Y. B. Chen, J. Wen, S.-C. Li, *Nano Lett.* **2018**, *18*, 6585-6590.

[23] a) X. Gonze, F. Jollet, F. Abreu Araujo, D. Adams, B. Amadon, T. Applencourt, C. Audouze, J. M. Beuken, J. Bieder, A. Bokhanchuk, E. Bousquet, F. Bruneval, D. Caliste, M. Côté, F. Dahm, F. Da Pieve, M. Delaveau, M. Di Gennaro, B. Dorado, C. Espejo, G. Geneste, L. Genovese, A. Gerossier, M. Giantomassi, Y. Gillet, D. R. Hamann, L. He, G. Jomard, J. Laflamme Janssen, S. Le Roux, A. Levitt, A. Lherbier, F. Liu, I. Lukačević, A. Martin, C. Martins, M. J. T. Oliveira, S. Poncé, Y. Pouillon, T. Rangel, G. M. Rignanese, A. H. Romero, B. Rousseau, O. Rubel, A. A. Shukri, M. Stankovski, M. Torrent, M. J. Van Setten, B. Van Troeye, M. J. Verstraete, D. Waroquiers, J. Wiktor, B. Xu, A. Zhou, J. W. Zwanziger, *Comput. Phys. Commun.* **2016**, *205*, 106-131; b) M. Torrent, F. Jollet, F. Bottin, G. Zérah, X. Gonze, *Comput. Mater. Sci.* **2008**, *42*, 337-351.

[24] a) J. P. Perdew, K. Burke, M. Ernzerhof, *Phys. Rev. Lett.* **1997**, *78*, 1396-1396; b) S. Grimme, J. Antony, S. Ehrlich, H. Krieg, *J. Phys. Chem.* **2010**, *132*, 154104.

[25] www.abinit.org, **accessed 20/3/19**.

[26] M. Methfessel, A. T. Paxton, *Phys. Rev. B* **1989**, *40*, 3616-3621.

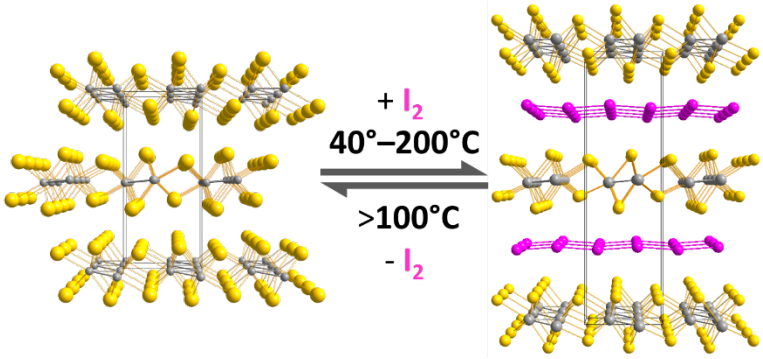

Patrick Schmidt, Philipp Schneiderhan, Markus Ströbele, Carl Romao, H.-Jürgen Meyer

Page No. – Page No.

Reversible Iodine intercalation into Tungsten Ditelluride